CHEMISTRY
A EUROPEAN JOURNAL

DOI: 10.1002/chem.200600172

Three-Phase Interlines Electrochemically Driven into Insulator Compounds: A Penetration Model and Its Verification by Electroreduction of Solid AgCl

Wei Xiao,[a] Xianbo Jin,*[a] Yuan Deng,[a] Dihua Wang,[a] and George Z. Chen*[a, b]

Abstract: A dynamic three-phase interline model has been developed for the reduction of a solid insulating metal compound to the metal in a suitable electrolyte, focusing on the electrochemically driven penetration of the process (or the three-phase interlines) into the insulator. Consideration is given to the effects of electrochemical, concentration and ohmic polarizations in the reduction-generated porous metal layer on top of the solid compound. Under potentiostatic conditions, reduction in the depth direction (penetration) becomes progressively slower as a result of the rising ohmic and concentration polarizations, whilst the electrochemical polarization exerts a declining effect. The quantitative equations established here also provide simple methods for the determination of some kinetic parameters of the reduction process, including ρ (total resistivity) and D_R (diffusion coefficient). The model has been experimentally verified by electrochemical reduction of solid AgCl with two novel metal|AgCl cylinder electrodes in aqueous solutions.

Keywords: electrochemistry · interfaces · kinetics · reduction · solid-state reactions

Introduction

Electrochemistry and relevant technologies can and should play important roles in provision of energy and materials to sustain the continuous improvement of the quality of life. Indeed, there has been continuous demonstration of innovations in laboratories, such as dye-sensitising TiO_2 to harvest solar energy[1] and electro-deoxidising TiO_2 to produce titanium metal.[2] However, great challenges still remain to commercialise some historical concepts, including the direct and efficient conversion of fuels to electricity in fuel cells[3] and the one-step and economical electrowinning of silicon from an electrolytic bath of molten salts.[4] There are a vast number of practical lessons to be learned and analyzed, but a theoretical interconnection to all these technological aspects, if it exists, should be identified.

Modern electrochemistry has been established on phenomena and processes at and near the interface between a solid electronic conductor (electrode) and a liquid ionic conductor (electrolyte).[5,6] One of the most commonly used theoretical tools to describe an electrochemical process is the Butler–Volmer (B–V) equation, which correlates electrode reaction rate or current density i to the combined thermodynamic and kinetic driving force, which is termed as the electrochemical polarization η_{ct} for charge (electron) transfer at the electrode|electrolyte interface. In conjunction with the Nernst equation and Fick's laws, the B–V equation can accommodate the effect of mass transport of the reactant/product in the electrolyte, known as the concentration polarization η_c.[5,6] Another effect is the ohmic polarization η_{ohm} (also known as the iR drop) due to the resistance of the electrode–electrolyte circuit to the current flow. In experimental terms, the three polarizations sum up to the difference between the measurable or applied electrode potential E and the equilibrium electrode potential E_{eq}, or simply the overpotential ($\eta = |E - E_{eq}| = \eta_{ct} + \eta_c + \eta_{ohm}$).

However, for most electrode|electrolyte systems, an experimental reality is the relatively constant physicochemical nature of the two phases involved and the geometric stability of the electrode|electrolyte interface. Consequently, the ohmic resistance through the electrode–electrolyte circuit is

[a] W. Xiao, Dr. X. B. Jin, Y. Deng, Dr. D. H. Wang, Prof. Dr. G. Z. Chen
College of Chemistry and Molecular Sciences
Wuhan University, Wuhan, 430072 (P. R. China)
Fax: (+86) 27-6875-6319
E-mail: xbjin@whu.edu.cn
mel@whu.edu.cn
george.chen@nottingham.ac.uk

[b] Prof. Dr. G. Z. Chen
School of Chemical, Environmental and Mining Engineering
University of Nottingham, University Park
Nottingham NG72RD (UK)
Fax: (+44) 115-951-4115

or can be treated as an invariable. Hence, η_{ohm} is a linear function of i and can be either experimentally eliminated by convenient electronic designs (e.g., a positive feedback loop) or theoretically included as a linear term in the relationship between i and η (or E).[7] Hence, most, if not all, fundamental studies focus only on η_{ct} and η_c. In particular, the B–V equation has been established on the basis of $\eta = \eta_{ct} + \eta_c$.[5–7]

In many technological systems, such as those mentioned above, the electrode reactions involve not only the electronic and ionic conductor phases, but also a third phase that is electrochemically active but often insulating to both ions and electrons, such as the oxygen gas at the cathode in fuel cells and the solid TiO_2 at the cathode in electro-deoxidation cells. The insulator phase can only participate in the electrode reaction when it joins the electronic and ionic conductors to form a conductor|insulator|electrolyte three-phase interline (3PI). Therefore, it is important to understand whether the ohmic polarization of the electron-transfer process at the 3PI can still be treated in the same way as that at the two-phase interface.

If the length and location of the 3PI remained unchanged with progression of the electrode reaction, η_{ohm} could still be an unimportant factor, but this may not be the case in reality. In the oxygen gas cathode in fuel cells, electron transfer occurs at the gas|catalyst|electrolyte 3PI. Freshly prepared catalyst particles are a few nanometres in size. In a typical 1000 h of operation, the particles can grow larger by 50–100% of their original size, likely due to sintering.[8] As a result, variations occur in the total length and location of the gas|catalyst|electrolyte 3PI. The exact effect of these changes is still unknown, but to maintain the same current output from the fuel cell, localized increase in current density at and around the catalyst particles is expected, and this will in turn increase η_{ohm}. In the case of electro-deoxidation of TiO_2 or other solid metal oxides,[9–16] electron transfer takes place at the metal|oxide|electrolyte 3PI, whose length and location change continuously with progressing oxide-to-metal conversion. A more complicated variation of η_{ohm} is then anticipated.

These two practical examples raise the general theoretical question how η_{ohm} would affect electrode reaction(s) at a dynamic 3PI. With a broader view to various technological needs, the time has now come for electrochemical research to move from last century's focus on two-phase interfaces towards three-phase or multiphase interlines. A few pioneering studies have already appeared,[17–19] and this article, the first part of this work, places unprecedented emphasis on various polarizations, particularly η_{ohm}, at or next to the dynamic 3PIs through both theoretical derivation and experimental confirmation by using two novel metal|AgCl cylinder electrodes in aqueous solutions. The second part of this work, to be reported elsewhere, applies the penetration 3PI model presented below to the electroreduction of solid SiO_2 to pure Si in molten $CaCl_2$, which promises green production of silicon.[11,19–21]

The Model

Basics of electrochemistry at 3PIs: Consider a macroscopic cylinder of an insulator metal compound MX which can be electrochemically reduced according to reaction (a).

$$\begin{aligned} &\mathrm{MX\ (solid\ compound)} \\ &+z\,\mathrm{e} \rightarrow \mathrm{M\ (solid\ metal)} + \mathrm{X}^{z-}\ \mathrm{(in\ electrolyte)} \end{aligned} \qquad \text{(a)}$$

The cylinder is electrochemically insulated on its sidewall with one of its end faces exposed to a liquid electrolyte. A wire mesh of the metal (or an inert metal), functioning as the current collector, is in contact with the exposed end face, as illustrated in Figure 1a. Under a sufficient negative

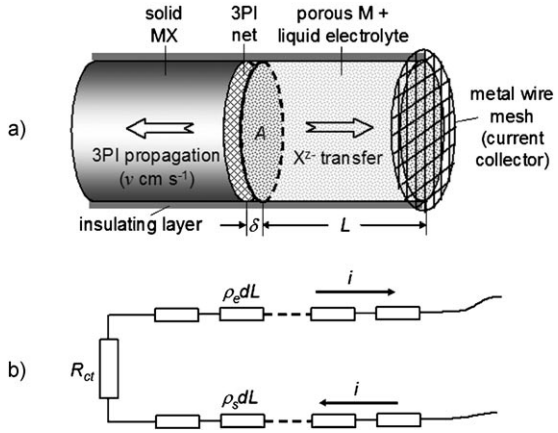

Figure 1. a) Schematic electrochemical reduction of an insulating solid-cylinder electrode via the penetration of M (metal)|MX (compound)|electrolyte three-phase interlines (3PIs). b) Electric-circuit simulation of a) in which R_{ct} is the charge-transfer resistance, and ρ_e and ρ_s are respectively the resistivities of the solid phase and the solution phase in the reduction-generated porous metal layer.

potential, reduction will start at the initial current collector|MX|electrolyte 3PIs. When the compound is reduced, the X^{z-} ion moves into the neighbouring electrolyte solution and is transported to the bulk electrolyte. The reduction-generated metal M should be porous due to the decrease in molar volume from MX to M. Simultaneously, the electrolyte solution enters the pores, leading to the formation of new M|MX|electrolyte 3PIs. The reaction then continues at the newly formed 3PIs until the electrode is completely reduced.

At an arbitrary reduction depth L (cm), there are many 3PIs between the MX and M phases. These 3PIs interconnect into a net with an apparent reaction area A (cm^2) and extend to a small thickness of δ (cm). Thus, the total reduction of the solid electrode can be described as the penetration of the 3PIs or the inward movement of the 3PI net (Figure 1a). The movement rate v ($cm\,s^{-1}$) of the 3PI net is defined as $v = dL/dt$. From Coulomb's Law, the measured total current I can be correlated to the movement rate v by Equation (1), where t (s) is the time and q ($C\,cm^{-3}$ or $A\,s\,cm^{-3}$)

the charge needed to reduce a unit volume of MX to M, which can be calculated from the formula mass and density of MX.

$$I = \frac{dQ}{dt} = qA\frac{dL}{dt} = qAv \quad (1)$$

For an electrochemical process at a stationary electrode|electrolyte interface, the current density i on the electrode is determined by the overpotential $\eta = |E - E_{eq}|$, according to the B–V equation. An important assumption for establishing the B–V equation is zero or negligible ohmic polarization η_{ohm} due to the electrode–electrolyte circuit resistance. In practice, the electrode–electrolyte circuit resistance is not always negligible, but the B–V equation can still be applied, after simple correction, to many stationary electrode|electrolyte interfacial systems. This is because the distance between the electrode|electrolyte interface and the other electrode always remains constant, and so does the electrode–electrolyte circuit resistance.

However, in the dynamic 3PI system depicted in Figure 1, the resistance of the electrolyte contained in the reduction-generated porous metal layer will increase continuously as reduction proceeds inwards from the end face of the cylinder. This situation is shown in Figure 1b, which is the electric-circuit representation of the electronic and ionic conduction by two rails of serially connected resistors, joined at the reaction resistor. During reduction, the potential-driven electrons flow through the porous M to the 3PIs and combine with MX (or M^{z+}) there. To maintain neutrality, the X^{z-} ions are rejected from the MX phase and move away from the 3PIs through the electrolyte in the pores of the porous M phase. The solid and solution resistivity in the formed porous metal layer are represented by ρ_e and ρ_s, respectively. Denoting a total resistivity ρ $(=\rho_e+\rho_s)$, the ohmic resistance R_{ohm} in the porous layer at the reaction depth L is given by Equation (2).

$$R_{ohm} = \rho L/A \quad (2)$$

Thus, R_{ohm} is a function of the reduction depth L and hence of the reaction time t. Then, if the total current flow is I, the overall ohmic polarization η_{ohm} can be expressed as Equation (3).

$$\eta_{ohm} = IR_{ohm} = \rho iL \quad (3)$$

By convention, the current density i and the exchange current density i^0 are both defined against the apparent area A of the cross section of the cylinder in Figure 1a. Consequently, a correction can be made to the B–V equation to include the ohmic polarization η_{ohm} [Eq. (4)]

$$i = i^0 \exp\left[\frac{\alpha nF(\eta-\eta_{ohm})}{RT}\right] - i^0\frac{C_R^s}{C_R^0}\exp\left[\frac{-\beta nF(\eta-\eta_{ohm})}{RT}\right] \quad (4)$$

where $\alpha(=1-\beta)$ is the charge-transfer coefficient for reduction, and C_R^s and C_R^0 are the concentrations of X^{z-} next to the 3PIs and in the bulk solution, respectively.

In this work, it is assumed that the solution contains sufficient supporting electrolyte to eliminate the effect of electromigration of the X^{z-} ions. Also, variations of the solution resistivity, the diffusion coefficient and the activity coefficient caused by the concentration change of X^{z-} are assumed to be negligible. Combination of the above equations leads to a new differential equation which will be highly challenging, if not impossible, to solve because C_R^s is a variable associated closely with the electrolysis conditions. In the following discussion, we provide approximate solutions to this equation for constant-potential electrolysis or potentiostatic conditions.

Note that although Equation (4) differs from the B–V equation only by the variable term η_{ohm} as a correction to the overpotential, it has never been considered as a nonlinear function of the current in any electrochemical system, either theoretically or experimentally. More importantly, as will be shown below, under particular conditions, Equation (4) in combination with Equations (1) and (3) can be simplified to different forms and hence predicts various simple and complex outcomes of theoretical and/or practical importance.

Potentiostatic electrolysis: In potentiostatic electrolysis or chronoamperometry, consider a sufficiently small increase in the reduction depth δL after the time needed for the establishment of steady-state diffusion of X^{z-} in the solution. It is then reasonable to assume an approximately linear concentration distribution of X^{z-} in the porous layer (Figure 2).

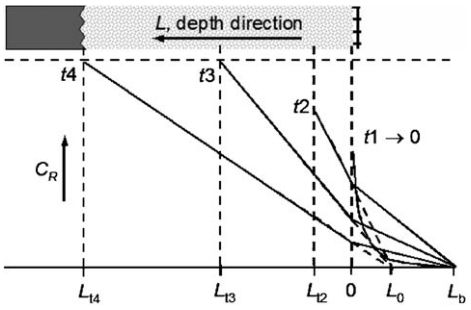

Figure 2. Schematic illustration of the approximate concentration distributions of the reduction-generated anions at different reaction times during potentiostatic electroreduction of a solid compound (cf. Figure 1). L_b and L_0 are the practical and effective thickness of the diffusion layer in the bulk solution, respectively.

This assumption can be mathematically verified for most situations with diffusion coefficients of about $10^{-5}\,cm^2s^{-1}$. The total thickness of the diffusion layer should be $L+L_b$ (Figure 2), where L_b is the thickness of the diffusion layer in the bulk solution. For a simplified consideration, an effective thickness L_0, as shown in Figure 2, is defined here to represent a linear extension of the anion distribution from the interior of the porous layer to the bulk solution. Then, Equation (5) applies, where D_R is the diffusion coefficient of X^{z-} in the solution in the pores of the porous metal layer.

$$i = zFD_R \frac{C_R^s - C_R^0}{L + L_0} \quad (5)$$

Introduction of Equations (3) and (5) into Equation (4) leads to Equation (6), in which the correlation between i, L and t, from Equation (1), can be expressed either as a differential equation or an integral [Eq. (7)].

$$i = i^0 \exp\left[\frac{\alpha nF(\eta - \rho iL)}{RT}\right] - i^0\left[\frac{i(L+L_0)}{zFD_R C_R^0} + 1\right]\exp\left[\frac{-\beta nF(\eta - \rho iL)}{RT}\right] \quad (6)$$

$$i = q\frac{dL}{dt} \text{ or } L = \frac{1}{q}\int_0^t i dt \quad (7)$$

Equations (6) and (7) together demonstrate, under a constant overpotential η, the correlations of reaction current i and reduction depth L with electrolysis time t. However, the simultaneous solutions of i and L are not simple with Equations (6) and (7).

To simplify the case, η can be divided into three terms: 1) electrochemical polarization η_{ct}, 2) concentration polarization η_c and 3) ohmic polarization η_{ohm}, as expressed by Equation (8).

$$\eta = \eta_{ct} + \eta_c + \eta_{ohm} \quad (8)$$

The concentration polarization η_c can be determined by combining the Nernst Equation and Equation (5) to give Equation (9), whereas η_{ct} is the potential deviation from η_c as the driving force for the reduction current.

$$\eta_c = \frac{RT}{zF}\ln\left(\frac{C_R^s}{C_R^0}\right) = \frac{RT}{zF}\left\{\ln\left[\frac{i(L+L_0)}{zFD_R C_R^0} + 1\right]\right\} \quad (9)$$

Case I: If $t \to 0$, then $L \to 0$ and η_{ohm} is very small. Equation (6) can be approximated as Equation (10) according to $\exp(-x) \approx 1 - x$.

$$i = \frac{i^0\left[\exp\left(\frac{\alpha nF\eta}{RT}\right) - \exp\left(\frac{-\beta nF\eta}{RT}\right)\right]}{1 + \frac{i^0 L_0}{zFD_R C_R^0}\exp\left(\frac{-\beta nF\eta}{RT}\right)} - \frac{i^0 iL\left[\frac{\alpha nF\rho}{RT}\exp\left(\frac{\alpha nF\eta}{RT}\right) + \frac{\beta nF\rho}{RT}\exp\left(\frac{-\beta nF\eta}{RT}\right) + \frac{1}{zFD_R C_R^0}\exp\left(\frac{-\beta nF\eta}{RT}\right)\right]}{1 + \frac{i^0 L_0}{zFD_R C_R^0}\exp\left(\frac{-\beta nF\eta}{RT}\right)} \quad (10)$$

From Equation (10), the product iL will approximately increase linearly as the current decreases [Eq. (11)], where a and b are constants for a given value of η and can be obtained by comparing Equation (10) with Equation (11).

$$i = a - biL \quad (11)$$

According to Equation (7), Equation (11) can be changed to a simple differential equation of L in correlation with t [Eq. (12)].

$$(1 + bL)q\frac{dL}{dt} = a \quad (12)$$

Introducing $t = 0$ and $L = 0$ as the initial conditions, Equation (12) has a unique analytical solution [Eq. (13)].

$$L = \sqrt{\frac{1}{b^2} + \frac{2at}{bq}} - \frac{1}{b} \quad (13)$$

Differentiation of Equation (13) against t leads to Equation (14).

$$i = \frac{a}{\sqrt{1 + 2abt/q}} \quad (14)$$

Case I will also hold in the following situations: 1) for very small η, then $i \to 0$; and 2) the system has negligible ρ (especially, $\rho = 0$). In both cases the product ρiL is very small.

Case II: According to Equation (14), when $t \to \infty$, $L \to \infty$ and i will be very small compared with its initial value. Consequently, the electrochemical polarization η_{ct} becomes negligible even for an applied large value of η. Under such a condition, Equation (15) applies.

$$\eta \approx \eta_c + \eta_{ohm} \quad (15)$$

In this case, the reaction rate will be mainly controlled by η_{ohm} and η_c, rather than Equation (6). The condition $L \to \infty$ also means $L \gg L_0$, that is, $L + L_0 \approx L$. Thus, by replacing η_c with $\eta - \eta_{ohm}$ and iL with η_{ohm}/ρ, Equation (9) is reorganized as Equation (16).

$$\frac{\eta_{ohm}^*}{\rho} = zFD_R C_R^0\left\{\exp\left[\frac{zF(\eta - \eta_{ohm}^*)}{RT}\right] - 1\right\} \quad (16)$$

For potentiostatic electrolysis, η is a constant. Therefore, solving Equation (16) will lead to a constant value of the ohmic polarization η_{ohm}^*. Then, combining Equations (3) and (7) gives Equation (17).

$$L\frac{dL}{dt} = \frac{\eta_{ohm}^*}{q\rho} \quad (17)$$

Assuming L_{min} to be the minimum reduction depth for Equation (16) to be valid (i.e., $L_{min} \gg L_0$), and t_{min} the time needed for the 3PIs to reach L_{min}, for $L > L_{min}$ or $t > t_{min}$, the initial conditions for Equation (17) can be written as $t = t_{min}$ and $L = L_{min}$. Then, the solution is Equation (18).

$$L = \sqrt{\frac{2\eta_{ohm}^*}{q\rho}(t - t_{min}) + L_{min}^2} \quad (18)$$

Differentiation of Equation (18) against t leads to Equation (19).

$$i = \frac{\eta^*_{ohm}}{\sqrt{\rho^2 L^2_{min} + 2\rho\eta_{ohm}(t-t_{min})/q}} \quad (19)$$

Equations (13), (14) and (18), (19) describe the theoretical penetration rates of the 3PIs at a given η for $t\rightarrow 0$ and $t > t_{min}$, respectively. According to the above discussions in both Case I and Case II, the physical image of the total reduction can be further demonstrated. With increasing t or L, the reduction current decreases. Accordingly, the electrochemical term η_{ct} decreases and, from Equation (8), $\eta_c+\eta_{ohm}$ will increase. However, because η_c and η_{ohm} are in correlation with the only variable iL [as shown in Eqs. (3) and (9)], they should change correlatively. In other words, they will both increase with L until η_{ct} becomes negligibly small, as shown in Equation (15). Then, both η_{ohm} and η_c reach their maximums, denoted as η^*_{ohm} and η^*_c, respectively, which should remain constant during further reduction. Thus, the product iL will also reach its maximum, denoted as $(iL)^*_\eta$ for an overpotential η, or as $(iL)^*_E$ for a potential E versus a reference electrode.

Figure 2 also shows the variation of C^s_R during potentiostatic electrolysis at different times. At the beginning ($t1\rightarrow 0$), the electrochemical polarization η_{ct} is very large due to a large reduction current. However, the concentration polarization η_c is relatively small (smaller C^s_R) although the concentration gradient is the largest (see the line for $t1$ in Figure 2). With the continuing reduction, L increases and η_{ct} decreases, leading to a greater concentration polarization (larger C^s_R). However, C^s_R will increase continuously to a constant when the reduction depth L becomes sufficiently large ($L \gg L_0$, see the lines for $t3$ and $t4$ in Figure 2).

In Case II, at a sufficiently large η, both η^*_{ohm} and η^*_c will be very large. From Equation (9), $C^s_R/C^0_R \gg 1$. Consequently, $\eta^*_c \approx \frac{RT}{zF}\ln\left[\frac{(iL)^*_E}{zFD_R C^0_R}\right]$. Then, for a given value of E, replacing η^*_{ohm} with $\rho(iL)^*_E$ and η with $|E-E_{eq}|$ in Equation (15) leads to Equation (20).

$$E = E_{eq} - \rho(iL)^*_E - \frac{RT}{zF}\ln\left[\frac{(iL)^*_E}{zFD_R C^0_R}\right] \quad (20)$$

Equation (20) shows the direct influence of the applied potential on the reduction rate (in terms of $(iL)^*_E$). However, for a more general situation, considering that E^0 is the potential of the $M|MX|X^{z-}$ electrode in equilibrium with an electrolyte containing 1 mol L^{-1} of the X^{z-} ion, and E and E^0 are referred to the same reference electrode, Equation (20) has a more common form [Eq. (21)].

$$E = E^0 - \rho(iL)^*_E - \frac{RT}{zF}\ln\left[\frac{1000}{zFD_R}(iL)^*_E\right] \quad (21)$$

Equation (21) can be directly used even for the situation where C^s_R is unknown. The kinetic parameters, such as ρ and D_R, can be obtained conveniently by nonlinear curve fitting to the experimentally measured values of E and $(iL)^*_E$ according to this simple equation. For example, at a given value of E, by plotting iL [$=iQ/(Aq)=IQ/(A^2q)$] against t, when $t > t_{min}$, iL will become a constant, that is, $(iL)^*_E$. Then, by plotting $(iL)^*_E$ against E and applying nonlinear curve fitting to the plot with Equation (21), ρ can be obtained directly, whereas D_R can be calculated with a known E^0.

Results and Discussion

Development of the 3PIs during potentiostatic electrolysis: As discussed above, from an initial electric contact point, the reduction of an insulating compound will develop along the surface and penetrate into the interior. These phenomena were observed with the Pt|AgCl electrode (see Experimental Section for details) during potentiostatic electrolysis in 0.5 mol L^{-1} HCl.

As shown in Figure 3, after electrolysis, a certain amount of AgCl around the Pt wire was converted to porous Ag, as observed by SEM. The expansion of the circular Ag|AgCl| electrolyte 3PI around the Pt wire on the electrode surface was fairly uniform in all directions (Figure 3a). Figure 3b is an SEM image of the electrolyzed Pt|AgCl electrode showing the reduction-generated porous Ag layer on top of the unconverted AgCl. The porous Ag layer should have allowed ingression of the electrolyte through the pores and then the formation of new inner Ag|AgCl|electrolyte 3PIs at the porous Ag|solid AgCl boundary. Removal of the porous Ag layer in HNO_3 (2 mol L^{-1}) resulted in a shallow depression on the end face (Figure 3c) with the Pt wire exposed in the centre. The reduction width W, defined as the radial expansion or displacement of the 3PI on the surface, was directly measured from the SEM image. The reduction depth L was also estimated from the length of the exposed Pt wire on a slanted (75°) SEM observation (Figure 3d). Figure 4 plots such measured W and L against the electrolysis time t.

As expected,[19] W increased approximately linearly with t, but this linear relationship was only maintained for several seconds at an overpotential of 200 mV, and a negative deviation followed (Figure 4a). The decrease of the expansion rate of the 3PI on the end surface may be attributed to the concentration polarization because of the difficulty of transferring the reduction-generated Cl^- through the reduction-formed porous Ag layer. (Mass-transfer kinetics were regarded to be absent in our recently reported thin-layer model.[19])

Figure 4b shows that the expansion of the 3PI on the surface was much faster than the penetration of the 3PIs in the depth direction. This phenomenon can be explained by the effects of η_c and η_{ohm} on the reduction of the interior AgCl according to Equations (13) and (18). Figure 5 highlights this difference by plotting the L/W ratio against the applied

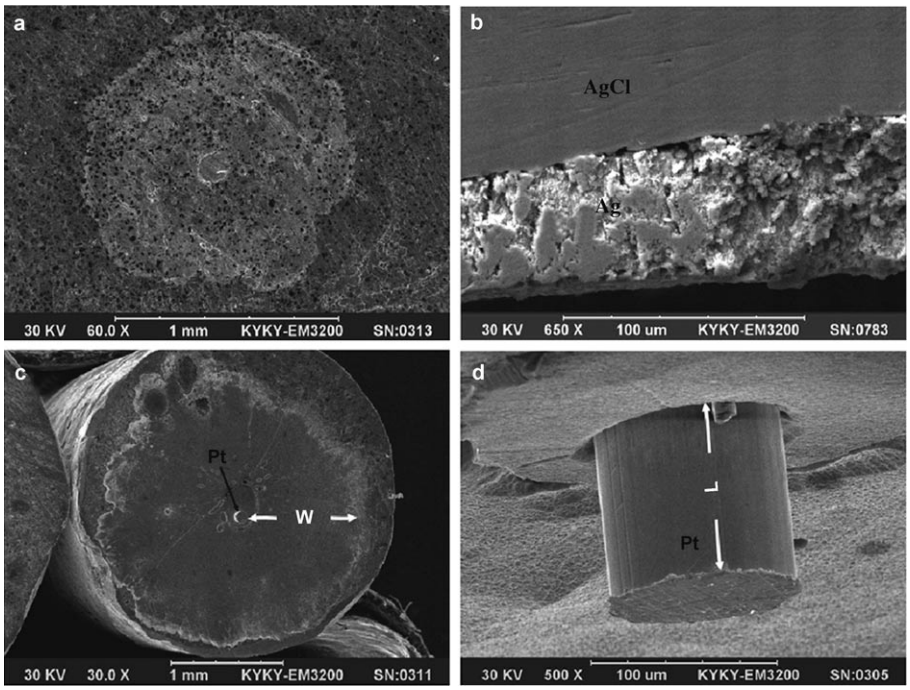

Figure 3. SEM observations on the Pt|AgCl electrode after potentiostatic electrolysis (−0.3 V in 0.5 mol L^{-1} HCl). a) Top view of the end face after 20 s of electrolysis. b) Sectional observation of a) after cutting with a surgical knife. c) Top view of a reduction-generated depression (60 s of electrolysis). d) Slanted (75°) observation of the exposed platinum wire in c).

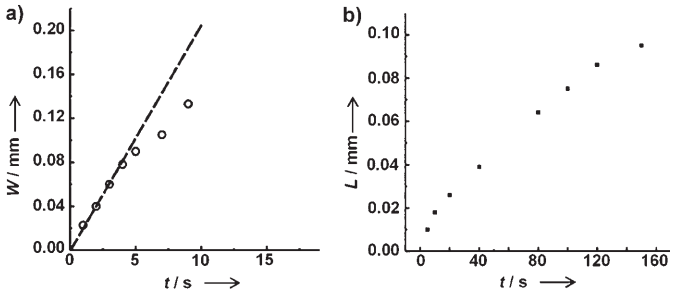

Figure 4. Typical results from potentiostatic electrolysis (−0.2 V) of the Pt|AgCl electrode at 300 K in 0.5 mol L^{-1} HCl showing the correlations of reduction width W (a) and depth L (b) with electrolysis time.

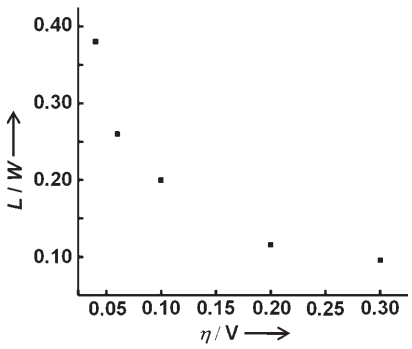

Figure 5. Correlation of the depth/width ratio L/W with the overpotential η; the width for each overpotential was the same ($W = 0.5$ mm).

η with W fixed at 0.5 mm. It can be seen that the L/W ratio is very small, especially at larger η. These results show that the reduction of inner AgCl is much more difficult, and penetration of the 3PIs in the depth direction would be a very influential step for the complete reduction of bulk metal compound. This aspect is further discussed in the next section.

High-polarization pretreatment of the Ag|AgCl electrode: As depicted in Figure 1a, to study the reduction in the depth direction, it is desirable to have an initial uniform contact between the current collector and the end face of the cylinder of the insulator compound. Such an initial uniform contact can be alternatively achieved by preformation of a uniform and thin layer of porous Ag at the end face of the AgCl cylinder. The results discussed above show that such a porous Ag layer would be very slow to form with the Pt|AgCl electrode because of the relative large area of AgCl at the end of the electrode. Therefore, the Ag|AgCl electrode, which had a much smaller area of AgCl at the end face, was used (see Experimental Section for details). The experiments were carried out in an electrolyte of 0.5 mol L^{-1} H_2SO_4 + 0.5 mmol L^{-1} HCl to minimise the influence of electromigration. Also, a larger overpotential should also help increase the rate of formation of the top Ag layer.

Figure 6a shows three I/t curves independently recorded on three new electrodes under the same polarization (−0.7 V versus AgCl|Ag). These almost identical plots indicate high reproducibility of the Ag|AgCl electrodes. In the initial 3 s, rapid growth of the current suggested fast increase in the total length of the 3PIs developing both in the transverse and the depth directions (see Figure 6b and c). When the surface 3PI expansion approached its maximum at the edge, the reaction could only progress in the depth direction; this accounts for the current drop after the peak. Before and at the current peak, the porous Ag layer could not be uniform in thickness. Close to the Ag wires L was larger than at the edge. Because η_c and η_{ohm} would be larger at longer L, the reduction in the depth direction should be slower near the Ag wires than near the edge. This difference in reduction rates should help to eventually eliminate the thickness difference of the porous Ag layer between locations near the Ag wires and at the edge. Figure 7 illustrates this argument.

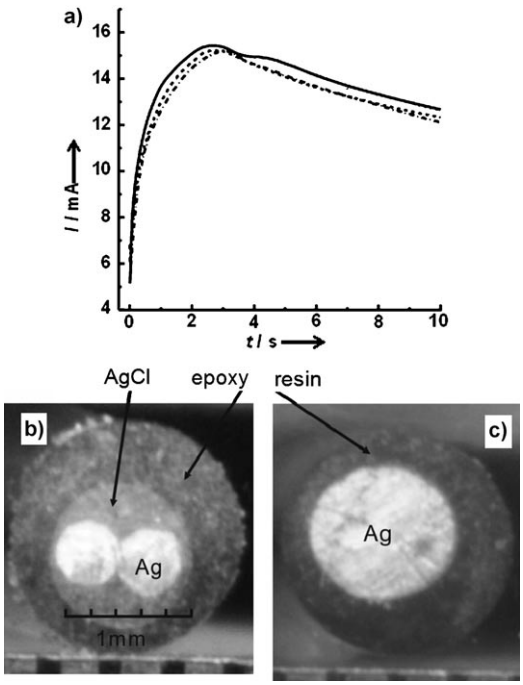

Figure 6. a) Three *I*/*t* curves recorded independently during chronoamperometric pretreatment of three new Ag|AgCl electrodes (−0.7 V in 0.5 mol L^{-1} H_2SO_4 containing 0.5 mmol L^{-1} HCl) and views of the end face of the electrode before (b) and after (c) pretreatment (polished).

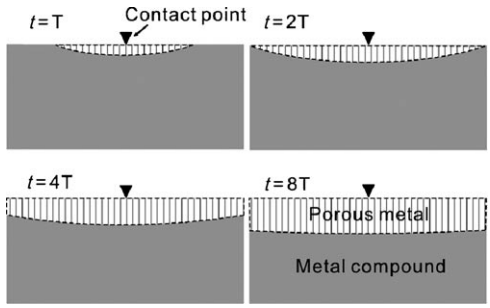

Figure 7. Schematic representation of the progression of the reduction of a solid compound along the surface ($t=T$ to $2T$) and the depth directions ($t=T$ to $8T$). T is an arbitrary time unit.

If the 3PI reaches the edge of the surface at time $2T$ (T is an arbitrary time unit), after a total reduction time nT, the reduction times and depths next to the Ag wires and near the edge of the end face will be respectively nT and L_{wire}, and $(n-2)T$ and L_{edge}. The difference between the two reduction depths ΔL can be estimated from Equation (18), which has the form of $L^2=At+B$ (where A and B are the collective constants). Hence, ΔL can be expressed as Equation (22).

$$\Delta L = L_{wire}-L_{edge} = \frac{L_{wire}^2-L_{edge}^2}{L_{wire}+L_{edge}} = \frac{2AT}{L_{wire}+L_{edge}} \leq \frac{2AT}{2L_{edge}} = \frac{AT}{\sqrt{A(n-2)T+B}} \quad (22)$$

Equation (22) indicates a longer reduction time (i.e., larger n) for a smaller ΔL. Particularly with small T (thin AgCl cylinder and higher overpotential), the difference in reduction depths can be eliminated quickly.

In the experiments, it was found that the pretreatment was very effective. Uniform L was observed visually after 10 s of pretreatment during careful and gradual polishing of the end face. During the course of polishing, the end face of the electrode became and remained metallically lustrous (Figure 6c) until the underlying grey AgCl suddenly and synchronously appeared.

Study on penetration of 3PIs in the depth direction: After pretreatment, the Ag|AgCl electrode resembles what is shown in Figure 1 and can be used to compare Cases I and II of the model. Figure 8a shows two typical *I*/*t* curves obtained from a pretreated Ag|AgCl electrode at two different overpotentials in 0.5 mol L^{-1} H_2SO_4 + 0.5 mmol L^{-1} HCl. These curves feature continuous decline of the current, that is, increasing η_c and η_{ohm} as reduction progresses inwards. The *I*/*t* curves of the Ag|AgCl electrode in 0.5 mol L^{-1} HCl were very similar in shape to those in 0.5 mol L^{-1} H_2SO_4 + 0.5 mmol L^{-1} HCl. However, it was thought that electromigration of the Cl^- ion could have occurred in 0.5 mol L^{-1} HCl, especially when a large overpotential was applied, and that, during reduction, the Cl^- concentration in the pores may vary significantly when the applied potential is changed, leading to different ionic strengths and hence different values of ρ and D_R at different potentials. To minimise these effects, the overpotential applied to the 0.5 mol L^{-1} H_2SO_4 + 0.5 mmol L^{-1} HCl solution was limited to 250 mV.

After each experiment, the colour change from AgCl to Ag was visible through the translucent epoxy resin sheath and allowed direct measurement of the reduction depth L with a micrometer calliper. Assuming reduction of AgCl to Ag to be the only electrode reaction, L can also be derived from the total charge Q (integration of I vs t) passed during pretreatment and chronoamperometric electrolysis via $L=Q/qA$. The L values calculated from Q agreed very well with those measured with the calliper at overpotentials between 200 and 450 mV (see Table 1), and this is evidence of the AgCl layer on the Ag wires being very uniform along the depth direction.

Table 1. Calculated and measured reduction depths on the Ag|AgCl|Cl^- electrode.

	Potential[a] [mV]					
	200	250	300	350	400	450
Q, pretreatment [C]	0.141	0.149	0.142	0.136	0.142	0.132
Q, electrolysis [C]	1.924	2.507	2.09	2.47	3.00	2.78
Q, total [C]	2.065	2.656	2.232	2.606	3.0142	2.912
L, calculated [cm]	0.128	0.099	0.107	0.125	0.145	0.140
L, measured [cm]	0.13	0.10	0.11	0.12	0.14	0.14

[a] The applied potential E was measured against the Ag|AgCl reference electrode in the same electrolyte and hence was the same as or close to the overpotential η in value.

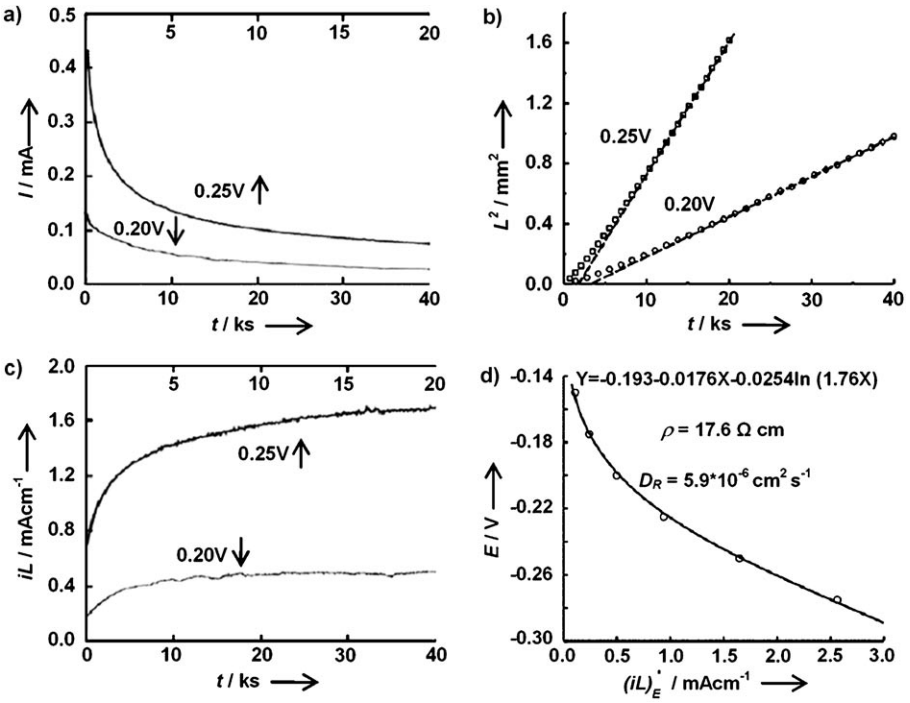

Figure 8. Chronoamperometric reduction of the Ag|AgCl electrode in the depth direction (in 0.5 mol L^{-1} H_2SO_4 + 0.5 mmol L^{-1} HCl). a) Typical *I*/*t* curves. b) Correlations of L^2 and *t*. c) Plots of *iL* against *t*. d) Correlation of the applied potential and $(iL)^*_E$; the solid line is the result of nonlinear curve fitting.

According to Equation (18), L^2 will vary linearly with *t* due to the increasing effects from the concentration and ohmic polarizations η_c and η_{ohm} after prolonged electrolysis (Case II), whereas Equation (13) holds in the initial period (Case I). This is fully supported by Figure 8b. In addition, Equation (18) is derived from the argument that the product *iL* should become invariable against *t* at later stages of electrolysis. Figure 8c verifies this argument by showing clearly that *iL* approaches a plateau after prolonged electrolysis.

Figure 8d plots the applied potential *E* against $(iL)^*_E$, where the values of $(iL)^*_E$ were calculated from the product of *IQ* at $L \approx 0.15$ cm for each *E*. Because E^0 is the potential of the Ag|AgCl|Cl^- electrode in equilibrium with a solution containing 1 mol L^{-1} Cl^- (see Equation (21) and the relevant text), the same electrode in the 0.5 mmol L^{-1} Cl^- solution should have an equilibrium potential that can be estimated to be $E^0 = \frac{RT}{F}\ln\left(\frac{0.0005}{1}\right) = -0.193$ V against the same reference electrode. By curve fitting according to Equation (21), the ohmic and concentration polarizations can be quantified by the two potential dependent terms $\rho(iL)^*_E$ and $\frac{RT}{zF}\ln\left[\frac{1000}{zFD_R}(iL)^*_E\right]$, respectively. The potential-independent parameters ρ and D_R were estimated from Figure 8d to be 17.6 Ω cm and 5.9×10^{-6} $cm^2 s^{-1}$, respectively.

The reliability of the above estimated values of ρ and D_R can be verified as follows. The use of two 0.5 mm silver wires as the current collector ensured insignificant electrical resistance. Thus, ρ should be mainly the solution resistivity in the pores. The resistivity ρ^0 of the 0.5 mol L^{-1} H_2SO_4 + 0.5 mmol L^{-1} HCl solution can reasonably be considered to be similar to that of 0.5 mol L^{-1} H_2SO_4 solution (5.05 Ω cm at 292 K[22]). The porosity of the silver layer generated from dense AgCl was measured previously to be about 60%.[23] For an actual porous electrode, the tortuosity coefficient λ is often greater than 1[24] and can be estimated from the solution resistivity ρ in the generated porous silver layer: $\lambda = 0.6\rho/\rho^0 = 2.09$. The tortuosity coefficient can also be calculated from the diffusion coefficient of Cl^- in the bulk solution: $D^0_R = 2\times10^{-5}$ $cm^2 s^{-1}$ at 298 K[24] and $\lambda = 0.6\,D^0_R/D_R = 2.03$. The very good accordance of the two differently calculated λ values with each other indicates that the estimated ρ and D_R are very reasonable.

Conclusion

A penetrating three-phase interline (3PI) model for the electrochemical reduction of an insulating solid compound to the solid metal, especially in the depth direction, has been established. Theoretical dynamic equations under potentiostatic conditions have been derived and verified by the electrochemical reduction of solid AgCl in aqueous solutions. It was found that reduction in the depth direction is much slower than that on the surface of the solid compound, and it determines the time for complete reduction. Under potentiostatic conditions, reduction in the depth direction is progressively slower as a result of increasing η_c and η_{ohm}.

The product of current and reaction depth ($iL = \eta/\rho$) increases with reduction time initially and then reaches a constant $(iL)^*_E$. A greater overpotential leads to larger $(iL)^*_E$ and also a faster reaction rate. From the developed theoretical relationship between *E* and $(iL)^*_E$, the diffusion coefficient D_R of the generated anion and the resistivity ρ (a mixture of the electrical and ionic terms) in the porous metal layer have been estimated.

Experimental Section

Electrode preparation

Pt|AgCl electrodes: The Pt|AgCl electrode was fabricated by inserting a Pt wire (∅ 100 μm) into molten silver chloride contained in a quartz tube (3 mm i.d.). After cooling, the Pt wire was fixed in the middle of the solidified AgCl cylinder which could be easily removed from the quartz

tube. The end face of the Pt|AgCl cylinder was manually ground until the Pt end was exposed, as illustrated in Figure 9a. During experiments, only the end part of this electrode was immersed in the electrolyte, and the electrochemical reduction began with the Pt end. The Pt|AgCl electrode is structurally similar to our previously reported W|SiO_2 electrode[19,20] for studying the reduction process on the surface of solid SiO_2 in molten $CaCl_2$.

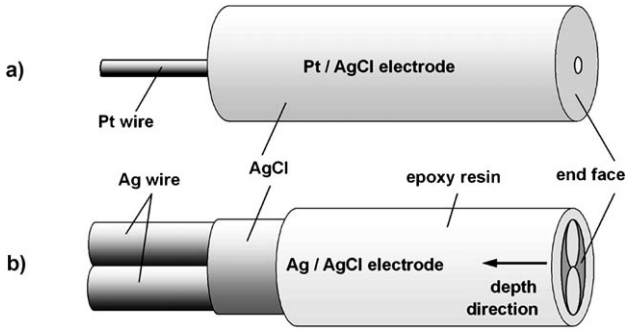

Figure 9. Schematic illustration of the designs of two metal|AgCl electrodes. a) Pt|AgCl electrode. b) Ag|AgCl electrode.

Ag|AgCl electrodes: To study the penetration of reduction into the interior of solid AgCl, the Pt|AgCl electrode was modified by replacing the thin Pt wire with two thicker Ag wires (∅ 0.5 mm). The Ag|AgCl electrode was also prepared in a thinner quartz tube (1.10–1.15 mm i.d., i.e., about twice that of the silver wire). Therefore, when the two silver wires were inserted into the quartz tube simultaneously, the space in the tube was divided approximately into two equal parts, which helped to form a uniform AgCl layer on both Ag wires during electrode preparation. After cooling, the electrode was removed from the quartz tube and then enclosed in a layer of epoxy resin to prevent current flow from the sidewall of the AgCl cylinder. The Ag|AgCl electrode is schematically illustrated in Figure 9b. Upon electrolysis, reduction started at the end face and then developed in the depth direction, as indicated in Figure 1a. Gravimetric analysis showed an even silver chloride coating (ca. 0.031 g-(AgCl) cm^{-1}) along the two silver wires. The end face had an apparent AgCl area of about 0.0056 cm^2. The value of q was calculated to be 3730 C cm^{-3}.

Electrochemical measurements: All experiments were conducted in a three-electrode cell (Figure 10). A porous silver disc served as the counterelectrode, and the Ag|AgCl reference electrode was coupled to the electrolyte via a Ruggin capillary containing the same electrolyte. Two aqueous electrolytes were used: 1) 0.5 mol L^{-1} HCl and 2) 0.5 mol L^{-1} H_2SO_4 + 0.5 mmol L^{-1} HCl.

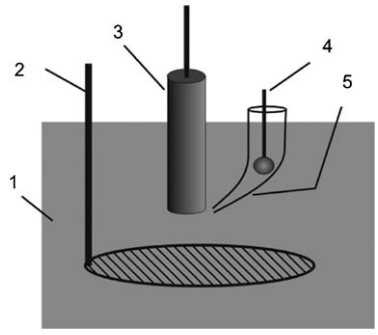

Figure 10. Schematic representation of the three-electrode cell used in this work. 1) Electrolyte, 2) silver counterelectrode, 3) working electrode, 4) Ag|AgCl reference electrode in the same working solution, and 5) Ruggin capillary.

Instrumentation and chemicals: Electrochemical data were recorded with a computer-controlled CHI660A Electrochemical System (Shanghai Chenhua, China). Electron microscopy was performed on a KYKY-EM3200 scanning electron microscope (SEM) (China). All chemicals were of analytical grade. Double- distilled water was used for making all aqueous solutions.

Acknowledgements

The authors are grateful to Professor J. T. Lu for useful discussions, and to the National Natural Science Foundation of China for financial support (Grant Nos: 20403012, 20125308 and 20573081). X.B.J and G.Z.C. also thank the Royal Society for the International Incoming Fellowships - China Fellowships (2005–2006).

[1] M. Gratzel, *Nature* **2001**, *414*, 586–587.
[2] G. Z. Chen, D. J. Fray, T. W. Farthing, *Nature* **2000**, *407*, 361–364.
[3] W. R. Grove, *Philos. Mag. Ser. 3* **1839**, *14*, 127–130.
[4] H. St. C. Deville, *Ann. Chim. Phys.* **1854**, *43*, 31–36.
[5] J. O'M Bockris, A. K. N. Reddy, M. Gamboa-Aldeco, *Modern Electrochemistry 2A—Fundamentals of Electrodics*, 2nd ed., Kluwer Academic/Plenum Publishers, New York, **2000**.
[6] A. J. Bard, L. R. Faulkner, *Electrochemical Methods: Fundamentals and Applications*, 2nd ed., Wiley, New York, **2001**.
[7] Z. W. Tian, *Electrochemical Research Methods*, Science Press, Beijing, **1984** (in Chinese).
[8] H. R. Colon-Mercado, H. Kim, B. N. Popov, *Electrochem. Commun.* **2004**, *6*, 795–799.
[9] G. Z. Chen, D. J. Fray in *Proceedings of the 6th International Symposium on Molten Salt Chemistry and Technology* (Eds.: N. Y. Chen, Z. Y. Qiao), Shanghai University, China, **2001**, pp. 79–85.
[10] K. Dring, R. Dashwodd, D. Inman, *J. Electrochem. Soc.* **2005**, *152*, E104-E113.
[11] T. Nohira, K. Yasuda, Y. Ito, *Nat. Mater.* **2003**, *2*, 397–401.
[12] X. Y. Yan, D. J. Fray, *Metall. Mater. Trans. B* **2002**, *33*, 685–693.
[13] G. Z. Chen, E. Gordo, D. J. Fray, *Metall. Mater. Trans. B* **2004**, *35*, 223–233.
[14] D. H. Wang, G. H. Qiu, X. B. Jin, X. H. Hu, G. Z. Chen, *Angew. Chem.* **2006**, *118*, 2444–2448; *Angew. Chem. Int. Ed.* **2006**, *45*, 2384–2388.
[15] A. J. Muir Wood, R. C. Copcutt, G. Z. Chen, D. J. Fray, *Adv. Eng. Mater.* **2003**, *5*, 650–653.
[16] G. H. Qiu, D. H. Wang, M. Ma, X. B. Jin, G. Z. Chen, *J. Electroanal. Chem.* **2006**, *589*, 139–147.
[17] M. Hermes, F. Scholz, *Electrochem. Commun.* **2000**, *2*, 845–850.
[18] U. Hasse, K. Wager, F. Scholz, *J. Solid State Electrochem.* **2004**, *8*, 842–853.
[19] Y. Deng, D. H. Wang, W. Xiao, X. B. Jin, X. H. Hu, G. Z. Chen, *J. Phys. Chem. B* **2005**, *109*, 14043–14051.
[20] X. B. Jin, P. Gao, D. H. Wang, X. H. Hu, G. Z. Chen, *Angew. Chem.* **2004**, *116*, 751–754; *Angew. Chem. Int. Ed.* **2004**, *43*, 733–736.
[21] W. Xiao, X. B. Jin, Y. Deng, D. H. Wang, X. H. Hu, G. Z. Chen, *ChemPhysChem* **2006**, *7*, 1750–1758.
[22] J. A. Dean, *Lange's Handbook of Chemistry*, 13th ed., Mcgraw-Hill: New York, **1985**.
[23] X. B. Jin, J. T. Lu, P. F. Liu, H. Tong, *J. Electroanal. Chem.* **2003**, *542*, 85–96.
[24] C. S. Cha, *Kinetics of Electrode Processes*, 3rd ed., Science Press: Beijing, **2002** (in Chinese).

Received: February 7, 2006
Revised: June 19, 2006
Published online: September 22, 2006

